

Propeller Cavitation Modelling by CFD - Results from the VIRTUE 2008 Rome Workshop

Francesco Salvatore¹, Heinrich Streckwall², Tom van Terwisga³

¹Italian Ship Model Basin (INSEAN), Rome, Italy

²Hamburg Ship Model Basin (HSVA), Hamburg, Germany

³Maritime Research Institute of Netherlands (MARIN), Wageningen, / Delft University of Technology, The Netherlands

ABSTRACT

Results from the Rome 2008 Workshop on cavitating propeller modelling are presented. Seven computational models by RANS, LES and BEM are benchmarked against a common test case addressing the INSEAN E779A propeller in uniform flow and in a wakefield. Submitted results provide a wide picture about capabilities of solvers based on different discretization techniques, turbulence and two-phase flow models. The comparative analysis of numerical results highlights a good agreement for the non-cavitating steady flow predictions, whereas for the cavitating flow, discrepancies in cavity extent are observed. In the case of a propeller operating in a non-uniform flow, difficulties to correctly model the inflow to the propeller are reflected in the differences in non-cavitating pressure distributions on the blade and hence in the transient cavity patterns.

Keywords

Marine Propellers, Cavitation, Multi-phase Models, RANS, LES, BEM, CFD Validation.

1 INTRODUCTION

During recent years Computational Fluid-Dynamics (CFD) models have demonstrated to rapidly become effective tools to analyse marine propeller single-phase flows. In contrast to this, cavitation presents complex two-and multi-phase flow phenomena that are still difficult to accurately simulate. In particular, cavitation nuisance like erosion, pressure fluctuations and noise are hardly captured by CFD-based solvers.

In this framework, the primary aim of the EU-FP6 Research Project 'VIRTUE, *The Virtual Tank Utility in Europe*' (www.virtual-basin.org) is to develop and assess multi-phase flow models for the analysis and design of marine propulsors. One of the five work packages of the VIRTUE Project, '*The Virtual Cavitation Laboratory*,' is devoted to this topic.

In October 2007, project partners involved into this Work Package organized a workshop to review the progress achieved in cavitation modeling by CFD. Results from

this Workshop, held at Wageningen, The Netherlands, are summarized by Streckwall and Salvatore (2008).

The present paper offers a review of the second workshop, held in October 2008, in Rome, Italy. As in the Wageningen 2007 Workshop, aim of the Rome 2008 Workshop is to analyse the performance of computational models to describe cavitating propeller flows. To compare results from different models, common test cases were proposed, and experimental results were made available to Workshop participants beforehand. Relevant flow features to be described by the CFD models were known *a priori* and computational set-ups could thus be adjusted to achieve the best performance with the computational models used. Thus, the numerical results from the workshop yield a clear picture of capabilities of different solvers, allowing for an analysis of weaknesses and strengths of computational models and identifying areas where further developments are required.

A cavitating propeller in "behind" conditions (that is operating in a non-uniform wakefield) was to be simulated. The Rome 2008 Workshop also proposed preceding test cases with a limited amount of geometrical/onset flow complexity: (i) a two-dimensional NACA 0015 foil, (ii) a three-dimensional twisted hydrofoil, that are not addressed here. Scope of this paper is to review test cases describing a propeller in a uniform inflow (Case A) and in a non-homogeneous wakefield (Case B). Common case definition reflects existing experimental data describing the INSEAN E779A model propeller tested at the Italian Navy Cavitation Tunnel (CEIMM, Rome, Italy), see Pereira et al (2004a, 2004b).

Propeller flow studies submitted by seven organizations (five from VIRTUE partners and two external to the project) allowed for a comparison of five solvers based on Reynolds-averaged Navier-Stokes (RANS) equations, one Large-Eddy Simulation (LES) model and one inviscid-flow Boundary Element Method (BEM). In the following sections, the proposed test cases are described and a brief overview of the computational models is given. Subsequently, the corresponding numerical results

submitted by workshop participants are compared and discussed.

2 THE PROPELLER FLOW TEST CASE

The INSEAN E779A propeller is chosen as reference case for the CFD benchmark exercise. A comprehensive series of experimental data addressing the propeller in a uniform as well as in a non-homogeneous flow is available for this propeller from an experimental programme performed at INSEAN over the last decade. Description of the INSEAN E779A experimental dataset may be found, e.g. in Pereira et al. (2004a) and Pereira et al (2004b).

2.1 Propeller geometry and test case definition

The INSEAN E779A is a four-bladed, fixed pitch, right-handed propeller, originally designed in 1959. Blade skew and rake are small, and pitch ratio is almost constant along radius ($P/D=1.1$). A bronze model of diameter $D_p=227.27$ mm is used for experimental work, Fig. 1. Geometry details are given in Salvatore et al (2006a).

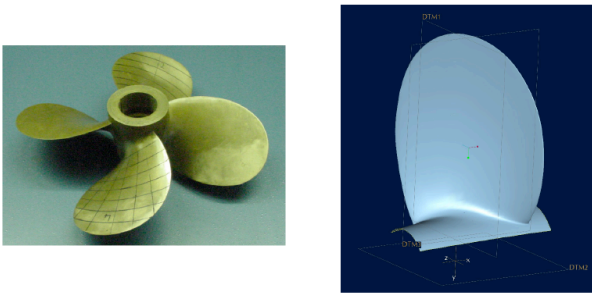


Figure 1. The INSEAN E779A model propeller ($D_p=227.27$ mm) and mathematical description of one blade (IGES).

In spite of a rather obsolete geometry typical of a 1950' design, the E779A propeller represents a challenging test case for validation of propeller codes and in particular, of cavitation models. For the Workshop purposes, the following operating conditions are considered:

- (A) uniform flow at speed $V = 5.808$ m/s and propeller rotational speed $n = 36.0$ rps (advance coefficient $J = V/nD = 0.71$); non-cavitating and cavitating flow at $\sigma_n = (p-p_v)/\frac{1}{2} (nD)^2 = 1.763$;
- (B) non-homogeneous flow at at speed $V = 6.22$ m/s and propeller rotational speed $n = 30.5$ rps ($J = 0.90$); non-cavitating flow and cavitating flow at $\sigma_n = 4.455$.

To achieve consistency among different numerical studies presented at the Workshop, a common description of propeller geometry in IGES format is provided to all participants. Similarly, a common definition of the computational domain is proposed. Experimental conditions reflect measurements performed at the Italian Navy Cavitation Tunnel (CEIMM, Rome, Italy). This tunnel has a squared test section of width 0.6 m and length 2.6m. To simplify the computational modelling of propeller in uniform flow, an idealized tunnel having a circular cross section and identical sectional area as the

actual tunnel was proposed at the Wageningen 2007 Workshop. This solution is kept for test case specifications at the 2008 Workshop, as illustrated in Fig. 2, where also dimensions of the prescribed computational domain upstream and downstream propeller disc are given.

A common definition of boundary conditions is also proposed: prescribed velocity at inlet section, zero pressure at outlet section, and slip at tunnel walls. No-slip conditions are enforced on propeller and shaft surfaces. Kinematic viscosity is $\nu = 1.01e-6$ m²/s and onset flow turbulence level is 2%.

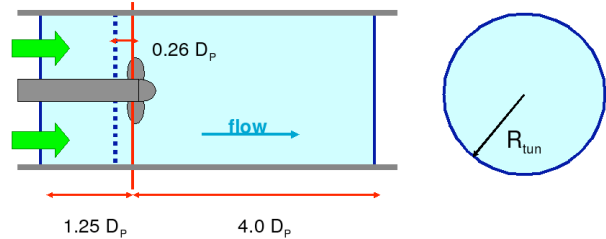


Figure 2. Idealized tunnel test section and dimensions ($R_{tun} = 1.471 D_p$).

2.2 Non-homogeneous inflow modelling

Workshop Case B is inspired to the INSEAN E779A dataset (Salvatore et al, 2006a), in which a non-homogeneous inflow is established through a wake generator placed upstream the propeller plane, Fig. 3. This physical set-up is used to approximately simulate a propeller operating behind a single-screw hull. To ensure a common definition of the non-homogeneous inflow to the propeller, no computational modelling of wake generator in the computational domain is requested, whereas suitable velocity boundary conditions at inlet section are imposed. This choice is motivated by the geometrical complexity of the wake generator. Numerical modelling of such a complex assembly might raise large discrepancies of wake generator wakefields resulting from different calculations, with uncontrolled consequences in propeller flow predictions.

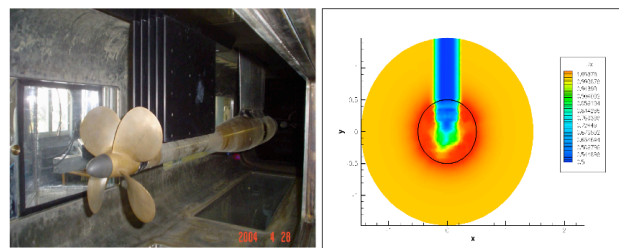


Figure 3. Propeller in non-homogeneous flow: tunnel set-up (left) and axial velocity distribution measured by LDV at section $x = -0.26 D_p$ used to prescribe velocity inlet conditions (right).

To overcome these problems, a common propeller inflow is defined through wakefield measurements by Laser-Doppler Velocimetry (LDV) at a transversal plane at distance $d = 0.26 D_p$ upstream propeller disc. Measurements without propeller (nominal wake) and with propeller (total wake) are available in the INSEAN E779A dataset, see Salvatore et al (2006a).

Axial velocity describing the LDV nominal wake is used to specify velocity conditions at inlet boundary ($x = -1.25 D_p$) for Workshop test case B, and no physical model of the wake generator is accounted for in the computational domain. Zero transversal velocity components along the inlet boundary are enforced.

3 SURVEY OF COMPUTATIONAL MODELS

Results submitted by seven organizations participating to the 2008 Workshop provide a wide spectrum of capabilities applied to marine propeller flow and cavitation modelling. Numerical solution of the Navier-Stokes equation is addressed by RANS (six participants), and by LES (one participant). As a term of comparison, numerical results by an inviscid-flow BEM solver including a sheet cavitation model are also considered.

3.1 Mathematical models and computational schemes

Computational models are briefly recalled here, whereas cavitation models are summarized in the next subsection.

Hamburg Ship Model Basin (HSVA, Germany) presents numerical studies by FreSCo, an incompressible unsteady RANS finite volume solver under development as a joint initiative between HSVA, the Maritime Research Institute of the Netherlands (MARIN), and the Technical University Hamburg-Harburg (TUHH). Transport equations are discretized with a cell-centred scheme and solved with a pressure-velocity coupling based on SIMPLE. The fully-implicit algorithm is second-order accurate in space and time. A standard $K-\omega$ turbulence model is used for present calculations. The solver is applied to unstructured grids using arbitrary polyhedral cells. Computational grids are obtained by using HEXPRESS, an automated grid generator. Details in Vaz & Hoekstra (2006) and Vorhölter et al (2006).

NUMECA Int. s.a, Belgium, presents results by its Commercial package FineTM/Turbo, a structured, density-based finite volume solver. Centered space discretization is employed with Jameson artificial dissipation. A four-stage explicit Runge-Kutta scheme is used for time discretization. Preconditioning is used to solve incompressible non-cavitating and cavitating flows. Present results are obtained by using a one-equation Spalart-Allmaras turbulence model, and computational grids are built by automated grid generators AUTOGRID 5 and IGG by NUMECA.

The Swedish Ship Model Basin (SSPA, Sweden) presents results by the commercial software FLUENT6.3, an unstructured cell-centred finite volume solver. Present calculations adopt its incompressible RANS formulation

and SIMPLE scheme, with a second-order QUICK scheme for convection terms and a second-order central difference for diffusion terms. The standard RNG $k-\epsilon$ turbulence model is used for the non-cavitating flows, whereas a modified RNG $k-\epsilon$ model is adopted for the prediction of cavitating flows. Further detail of using the latter approach can be found in Li and Grekula (2008).

VTT Technical Research Center of Finland presents numerical studies by FINFLO code, a finite volume solver based on the pseudo-compressibility method. Second order central-differencing is used for diffusion terms, whereas different upwind schemes are used for convection terms in steady, unsteady or cavitating flows. Time-integration is performed via approximate factorization and local time stepping. Present calculations adopt Chien's low-Re $K-\epsilon$ turbulence modelling, for details see Sánchez-Caja et al (1999).

The Applied Research Laboratory (ARL) from Pennstate University, Pennsylvania, USA, proposes a numerical study by the in-house code M-UNCLE, a cell-centered, finite volume solver based on a pseudo-compressibility formulation. Preconditioning is based on a second-order accurate dual-time scheme. Present calculations are performed through an incompressible flow assumption, and $K-\epsilon$, $K-\omega$ or DES turbulence models are employed. The computational domain is discretized by an overlapping structured grid approach (Kunz et al, 2000).

Chalmers University, Sweden, presents results by a cell-centered finite volume incompressible LES solver developed from OpenFOAM, the open source CFD library. The code adopts a velocity-pressure coupling by a PISO algorithm. The so-called mixed formulation is applied and dissipative subgrid modelling is accomplished via an implicit approach. Wall modelling is based on LES boundary layer equations and viscosity adaptation. Computational grids are unstructured, with tetrahedral cells away from walls and prisms in the boundary layer. See Bensow et al (2008) for details.

In addition to the above mentioned viscous-flow solvers, the Italian Ship Model Basin (INSEAN, Italy) contributes with results from an inviscid-flow model implemented through a Boundary Element Methodology (BEM) into the PFC-BEM code. An outline of this model is given in Pereira et al (2004a) and in Salvatore et al (2006b).

3.2 Cavitation models

Different cavitating flow models are implemented in RANS, LES and BEM solvers presented at the Workshop.

A single-fluid, single-phase barotropic model by Delannoy and Kueny (1990) is implemented in the FineTM/Turbo code. Density is constant in the pure liquid and pure vapor regions whereas it varies according to an equation of state $\rho=f(p)$ in the mixture region. Continuity and momentum equation for a single compressible fluid having density ρ are solved. A standard sine function law for $f(p)$ is used in the present work.

All the other Navier-Stokes solvers adopt multi-phase models based on a transport equation describing generation and evolution of vapor content in the fluid. Vaporization and condensation of vapor in respectively, cavity growth and collapse phases, are described through finite rate mass transfer models implemented via suitable source terms. This transport equation is solved in addition to mass and momentum equations for the mixture fluid. Alternative vaporization and condensation models characterize different multi-phase models addressed in the Workshop.

Chalmers' OpenFOAM and FINFLO codes adopt mass transfer models derived from an original approach proposed by Merkle et al (1998) and Kunz et al (2000) and implemented into the M-UNCLE code. Semi-empirical constants are used in the expressions of vapor production and destruction terms.

Cavitation models derived from isolated bubble dynamics via the Rayleigh equation are implemented in codes FreSCo and FLUENT 6.3. In particular, the formulation by Sauer (2000) is implemented in the FreSCo code, whereas the 'Full Cavitation Model' by Singhal et al (2002) is implemented in FLUENT 6.3.

Finally, an unsteady-flow sheet cavitation model is implemented into the PFC-BEM code. The approach is based on a cavity surface tracking model using the condition that flow pressure equals vapor pressure in the cavity. The methodology is valid only to address cavities attached to the blade surface.

3.3 Computational details

A summary of computational frameworks used to evaluate propeller flow by the Navier-Stokes solvers above is given in Table 1. Common to all RANS and LES models, propeller in uniform flow is studied in a rotating frame of reference fixed to propeller blades. Only one blade is explicitly considered and periodicity conditions are enforced. In most cases non-homogeneous inflow conditions are described by using a rotating grid block surrounding the propeller and fixed blocks for the remaining part of the computational domain. A sliding mesh technique is used at the interface between fixed and rotating blocks and governing equations are solved in the inertial frame. Numerical studies by Chalmers' OpenFOAM and FreSCo are performed by rotating the whole computational domain. This approach requires that inlet velocity distribution is interpolated at rotating grid cells at each time step.

As mentioned above, both structured and unstructured computational grids are used. The M-UNCLE code adopts an overlapping block technique. Propeller flow test cases A and B represent challenging grid generation exercises in that grid refinement at blade tip and along wake tip-vortex are necessary. The correct description of the non-homogeneous wakefield implies adequate modelling of the inlet region to avoid excessive numerical dissipation upstream the propeller. Furthermore, cavitation studies require that suitable grid cell clustering is made in flow

regions where vapor generation/destruction is expected to occur. Representative examples of structured and unstructured computational grids are given in Fig. 4.

Although trivial as compared to Navier-Stokes solvers, the computational set-up for BEM calculations is described for completeness. Inviscid-flow calculations by PFC-BEM are performed by assuming the propeller in an unbounded flow (no tunnel wall confinement effect described). Unsteady non-cavitating flow calculations proceed until periodic solution is achieved and then the cavitation model is switched on. Propeller surface discretization is chosen to minimize grid refinement effects and time discretization corresponding to angular step of 2.5 deg is used.

Code (organization)	Grid size wet/cav	Time-step / angular step	CPU effort
OpenFoam (Chalmers)	4.6 M	1.1E-6 s / 0.012 deg	
FreSCO (HSVA)	2.4 / 3.1 M	4.55E-5 s / 0.5 deg	3 days (8-proc)
Fine-Turbo (NUMECA)	3.0 / 11.4 M	2.28E-4 s / 2.5 deg	3 days (24-proc)
Fluent 6.3 (SSPA)	0.8 / 2.3 M	4.55E-4 s / 5 deg	
FINFLO (VTT)	1.7 / 5.9 M	4.55E-5 s / 0.5 deg	4 days (16-proc)
M-Uncle (ARL-PU)	3.7 / 7.3M	2.28E-5 s / 0.25 deg	0.6 days (192 proc)
BEM-PFC (INSEAN)	surface	2.5 deg	6 hours

Table 1. Summary of computational details.

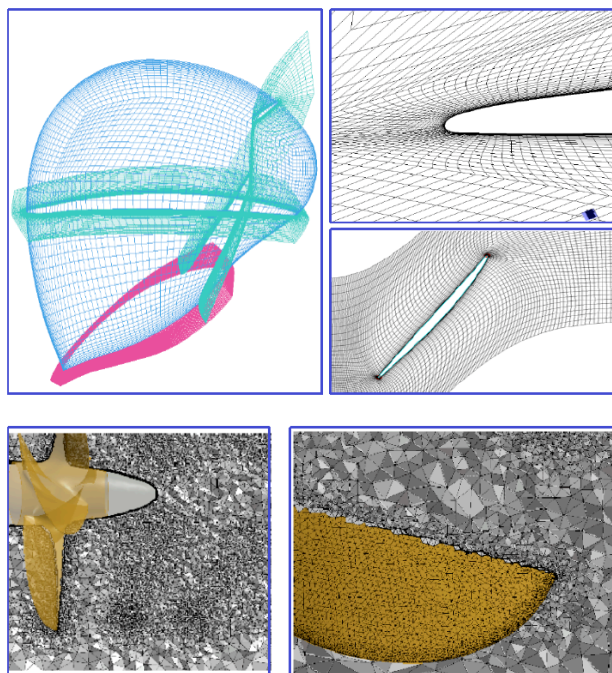


Figure 4. Examples of computational grid details. Structured grids (top) and unstructured grids (bottom).

4 NUMERICAL RESULTS: UNIFORM FLOW

The E779A propeller in uniform flow repeats a test case originally proposed at the Wageningen 2007 VIRTUE Workshop. In view of open issues left by the analysis of results submitted to the 2007 Workshop, this test case is proposed again for the 2008 Workshop, as a preliminary

step towards unsteady propeller flow calculations. Streckwall and Salvatore (2008) provide a detailed review of results presented at the 2007 Workshop.

4.1 Non-cavitating flow

First, non-cavitating conditions at the design point $J = 0.71$ are considered. Numerical predictions of propeller thrust and torque coefficients by all computational models are shown in Fig. 5. Experimental data from open water tests in towing tank are also shown for comparison. Evaluated thrust and torque coefficients are generally in fair agreement with experimental data over the considered range of advance coefficients J . Few cases present a rather constant offset from the average of computational results. As expected, inviscid-flow results by PFC-BEM correctly predict thrust, whereas torque is overestimated at high J and underestimated at low J .

Results for $J = 0.71$ are analysed in Table 2. Most of numerical model predict K_T and K_Q in close agreement with open water measurements. In fact, averaging the five best results out of seven, differences between measured and predicted thrust is 1.2% whereas the difference for torque is about 1%.

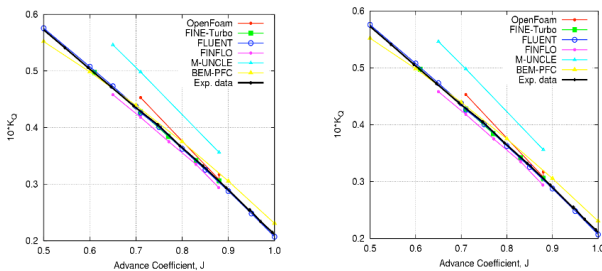


Figure 5. Uniform non-cavitating flow. Predicted propeller thrust and torque coefficients compared to O.W. data.

Table 2. Uniform flow, $J = 0.71$. summary of predicted thrust and torque coefficients and experimental data.

Uniform flow $J = 0.71$	Non-cavitating		Cavitating	
	K_T	$10 * K_Q$	K_T	$10 * K_Q$
Measured (tunnel)	0.256	0.464	0.255	0.460
Measured (O.W.)	0.238	0.429	-	-
FreSCo	0.237	0.438	-	-
Fine TM /Turbo	0.250	0.428	0.260	0.447
Fluent 6.3	0.240	0.426	-	-
FINFLO	0.234	0.418	0.249	0.459
M-UNCLE	0.276	0.498	0.256	0.476
Ch's OpenFOAM	0.256	0.453	0.252	0.450
PFC-BEM	0.244	0.419	0.247	0.449

The comparison with open water measurements is qualitative in that flow confinement effects are taken into

account in numerical calculations, with the only exception of BEM results. In the present case, confinement effects are estimated as 2% of both thrust and torque. For completeness, Table 2, gives also thrust and torque from cavitation tunnel measurements. Loads measured in the tunnel are about 8% higher than in open water, due to a particular calibration technique used. The comparison between numerical results and measurements from tunnel tests is presented in Fig. 6.

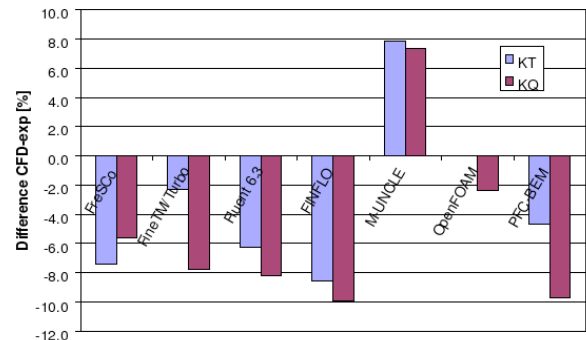


Figure 6. Difference in computed and measured thrust and torque coefficient for uniform flow conditions in tunnel @ $J=0.71$

The limited scatter among thrust and torque predictions is reflected by the comparison of pressure distributions on the blade surface. Figure 7 depicts pressure coefficient isosurfaces on blade suction side. All calculations detect a strong negative pressure peak in the leading edge region that is typical for this type of propellers with constant pitch distribution along radius. It should be noted that comparisons of results from different contour maps can be only qualitative in that slightly different color maps and levels are used. This comment holds for Fig. 7 below as well as for all contour plots shown hereafter.

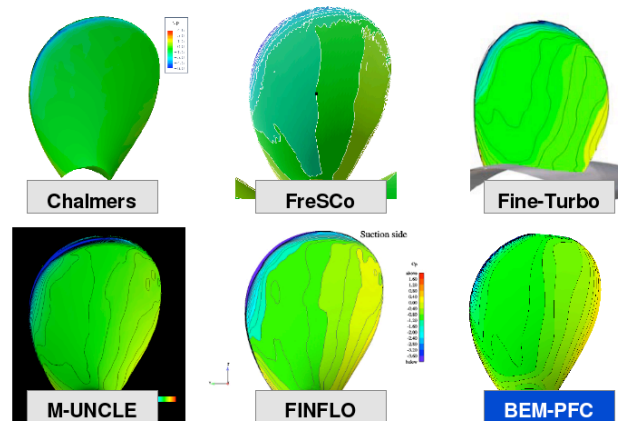


Figure 7. Uniform non-cavitating flow. Pressure isosurfaces on blade suction side.

To get a first impression of the cavity extent without invoking a cavitation model, it is interesting to analyse the flow domain where the pressure in wetted flow conditions

drops to values close to the vapor pressure. To this end, Fig. 8 illustrates isopressure contours at $C_p = -1.0$ in a flow region surrounding the blade suction side. It is noted this pressure criterion is supposed to show a larger volume (corresponding to $\sigma_n = 1.0$) than the cavitation number of $\sigma_n = 1.76$, which is discussed later. This type of result in terms of volume regions is typically not given by inviscid-flow BEM calculations where in first instance only flow quantities on the propeller surface are evaluated. Comparing the results of different codes, a region extending from mid-span leading edge to blade tip is clearly observed in all solutions. It is expected that vaporization mostly occurs in this area. Differences between the results from different codes become especially apparent in the tip region and the blade root region.

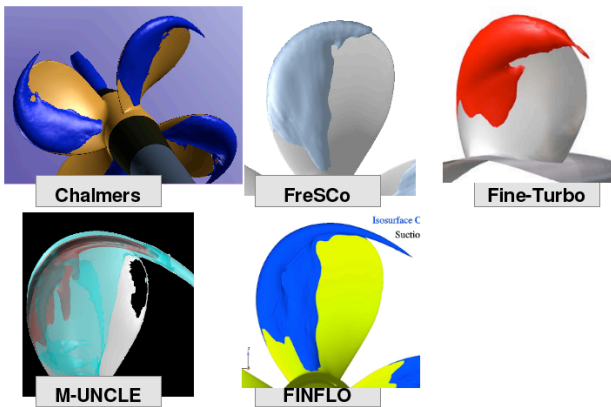


Figure 8. Uniform non-cavitating flow. Constant pressure contour for $C_p = -1.0$ on blade suction side predicted by viscous-flow solvers.

4.2 Cavitating flow

Cavitating flow conditions at the design point $J = 0.71$ and cavitation number $\sigma_n = 1.76$ are considered in the following. Pressure isosurfaces on blade suction side are shown in Fig. 9, whereas Fig. 10 compares predicted extensions of cavitating regions. Dealing with inviscid-flow BEM-PFC results, the cavity shape determined through a surface tracking technique is plotted. The irregular shape of the cavity trailing edge is a consequence of the comparatively coarse discretization of the blade surface. In viscous-flow calculations, cavity extension is assumed to be limited by vapor fraction contours with $\alpha_v = 0.5$. Although the correspondance between cavity and flow regions tagged by $\alpha_v = 0.5$ is open to discussion, the results from plots in Fig. 10 may be used to compare the extension of cavitating flow regions predicted by CFD codes with the results from experiments.

The comparison from Fig. 10 highlights that all computational models are qualitatively able to describe the basic features of the cavitating flow observed during the experiments. There is a fair correspondence in spanwise sheet cavity extent. All codes predict that the

cavity length increases rapidly from the inner to the outer radial stations and at the blade tip the cavity merges into a strongly cavitating tip-vortex. The cavity is attached to blade surface and stable, with very limited formation of clouds. This is confirmed by experimental data indicating a standard deviation of the measured cavity extension of only 2.5% of its mean extent (projected cavitating area). It is noted that all numerical predictions overestimate the cavity extension. This is true in particular for results by FINFLO and Chalmers' OPENFOAM where excessive vapor at blade mid-chord is detected. Tip-vortex cavitation is observed in results by M-UNCLE, Chalmers' OPENFOAM, and to a very limited extent by FRESCO. Reasons for these discrepancies are cavitation modelling, and the computational grid density in the tip-vortex region.

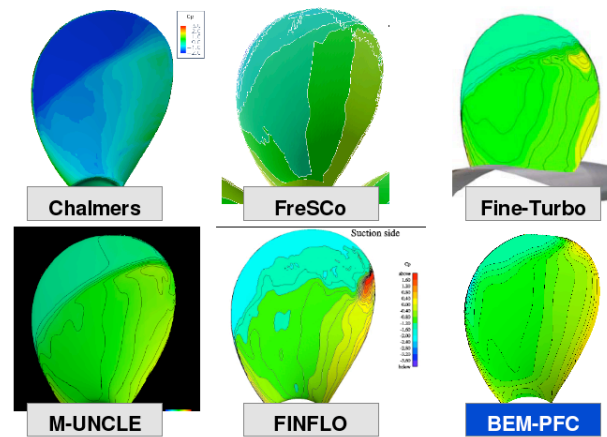


Figure 9. Uniform cavitating flow. Pressure isosurfaces on blade suction side.

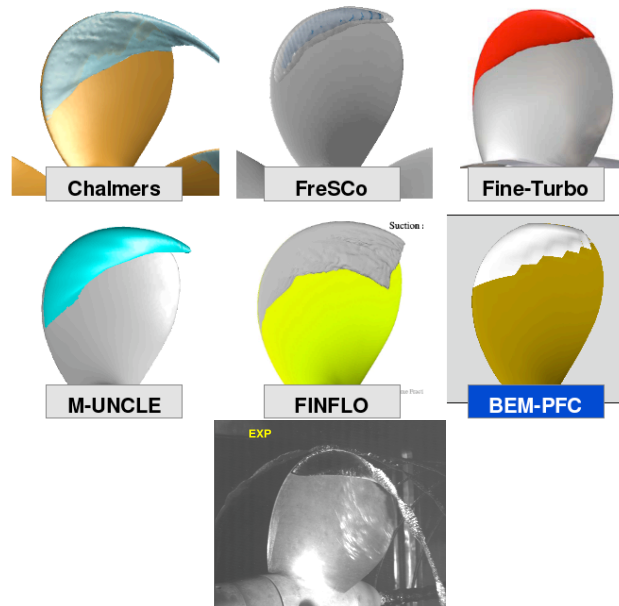


Fig. 10. Uniform cavitating flow. Vapor fraction contour for $\alpha_v = 0.5$ on blade suction side by RANS and LES solvers. Predicted cavity surface by BEM code and observed cavity pattern from experiments.

5 NUMERICAL RESULTS: UNSTEADY FLOW

The test case addressing the E779A propeller in non-homogeneous inflow is complicated by the necessity to ensure a correct description of the prescribed velocity distribution at the inlet section of the computational domain. As for the CFD models, the results from FLUENT, FINFLO and M-UNCLE are obtained by interpolating the prescribed velocity distribution from LDV measurements in the cavitation tunnel, see Fig. 11. A different approach is used in the calculations by Chalmers' OPENFOAM and FreSCo where an idealized velocity distribution approximating the LDV-based inflow in Fig. 3 is considered. Boundary conditions for inviscid-flow calculations by the BEM-PFC code are obtained by imposing a velocity distribution at propeller plane obtained through interpolation of LDV data.

To quantify the effect of different numerical descriptions of the incoming velocity field, a comparison of the axial velocity component on a transverse plane located at distance $d = 0.52 R$ upstream of the propeller disc is depicted in Fig. 11. Numerical results from RANS and LES solvers are compared here with experimental data by LDV. Although color maps are different between the various plots, large discrepancies in numerical results are apparent.

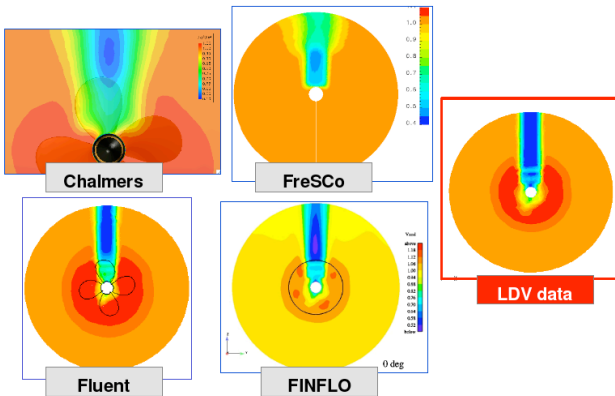


Figure 11. Axial velocity distributions at transversal plane at distance $d = 0.52 R$ upstream the propeller disc. Numerical results and experimental data by LDV.

5.1 Non-cavitating flow

Non-cavitating flow conditions at $J = 0.90$ are considered. The non-homogeneous wakefield incoming to the propeller and illustrated in Fig. 11 induces a periodic variation of the pressure on the blade surface, with high loadings occurring when the blade crosses the narrow wake peak where most of the velocity defect is concentrated (see Fig. 3).

Figure 12 shows pressure isosurfaces, on blade suction side for three blade angular positions: $\theta = -30, 0, +30$ deg, with $\theta = 0$ corresponding to the reference blade in the twelve o'clock position. Similarly, Fig. 13 shows isopressure contours for $C_p = -3.0$ on blade suction side for the same angular positions. Available results from

FreSCo, FINFLO, FINE-TURBO and BEM-PFC codes present a qualitative agreement in Fig. 12.

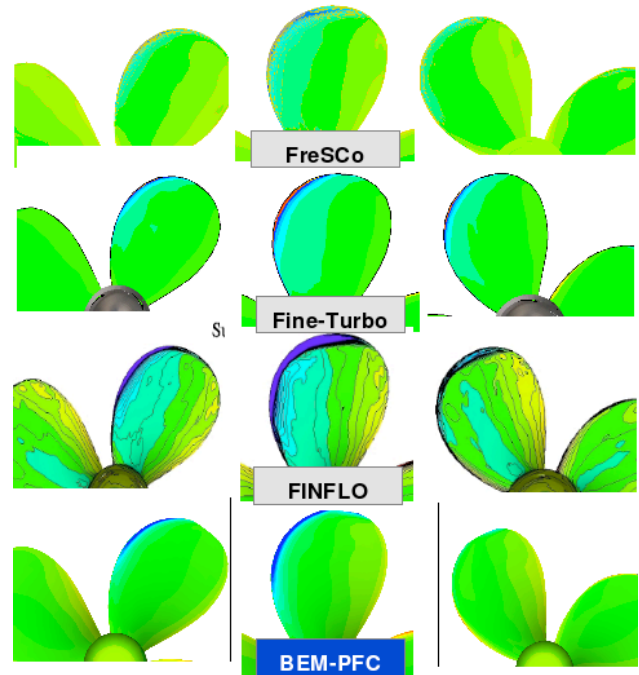


Figure 12. Unsteady, non cavitating flow. Pressure isosurfaces on blade suction side at blade angular positions $-30, 0, +30$ deg.

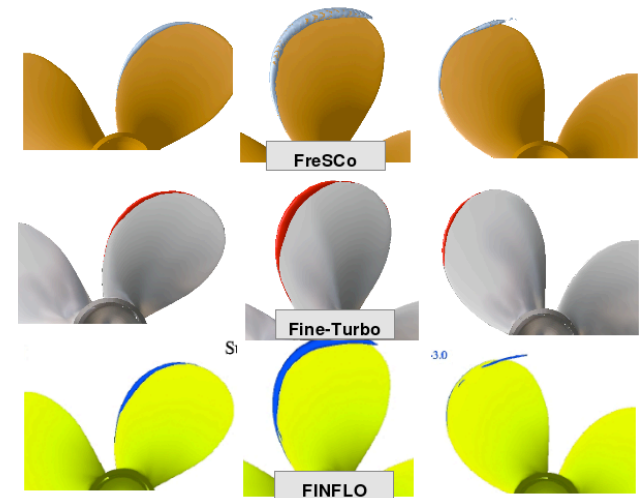


Figure 13. Unsteady, non cavitating flow. Constant pressure contour for $C_p = -3.0$ on blade suction side predicted by viscous-flow solvers. Blade angles $-30, 0, +30$ deg.

5.2 Cavitating flow

Cavitating flow conditions at $J = 0.90$, $\sigma_n = 4.455$ are considered. As a result of the periodic variation of blade loading, a transient cavitation is observed on the propeller blades. A sequence of snapshots describing the cavity pattern variation as observed from experimental visualizations is shown in Fig. 14. Frames are taken for

blade angular positions between -35 and +20 degrees, with angular steps of 5 degrees. Figure 15 illustrates predicted cavity extensions for three angular positions. Similarly to cavitating flow results shown in Section 4, viscous-flow results from the RANS and LES codes presented correspond to vapor fraction contours with $\alpha_v = 0.5$, whereas the actual cavity surface determined by the surface tracking technique coupled to the BEM method is used to describe results by the inviscid-flow code PFC.

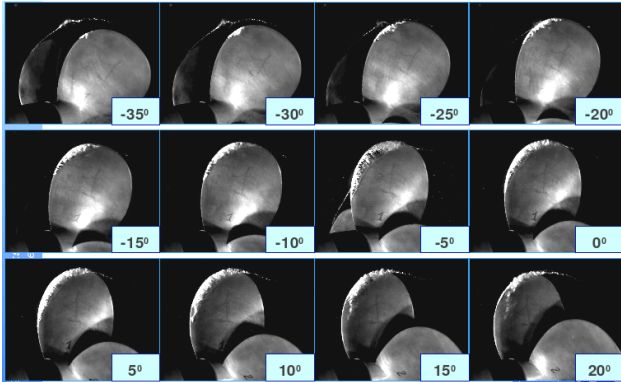
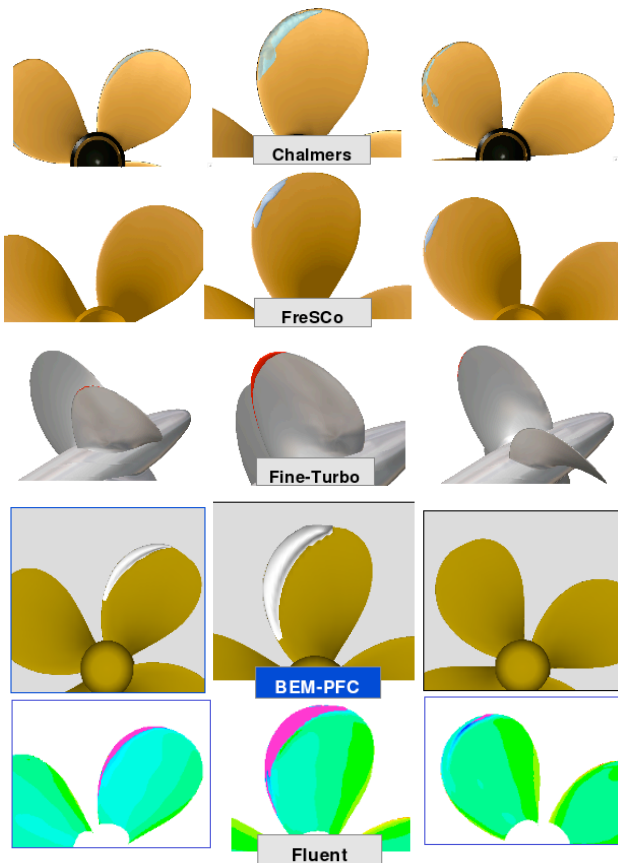


Figure 14. Sequence of snapshots describing cavity pattern variation as observed from tunnel visualizations. Blade angular positions between -35 and +20 degrees,



step 5 degrees.

Figure 15. Unsteady, cavitating flow. Vapor fraction contour for $\alpha_v = 0.5$ on blade suction side by RANS and LES solvers. Predicted cavity surface by BEM code. Angular positions -30, 0, +30 deg.

6. COMPARATIVE ANALYSIS OF CAVITATING FLOW PREDICTIONS

Let us first have a closer look at the cavitating propeller in a uniform flow. Combining results for the present test case from the VIRTUE 2007 Workshop with those submitted to the 2008 Workshop, a total of eleven different models can be compared. Predicted cavity patterns from RANS and LES code (isosurface $\alpha_v = 0.5$) and by BEM (evaluated cavity surface) are in Fig. 16.

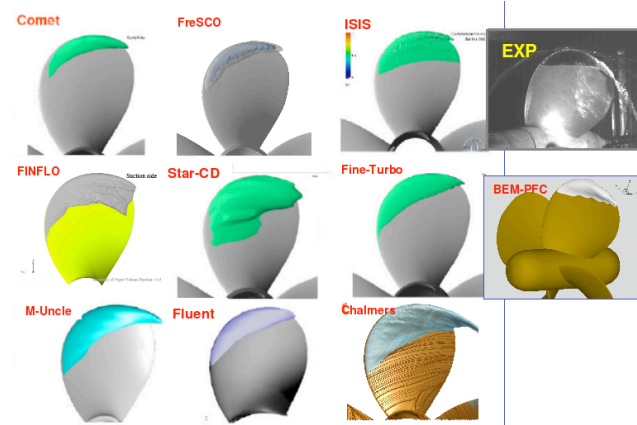


Figure 16. Uniform cavitating flow. Synopsis of predicted cavity patterns from VIRTUE 2007 and 2008 Workshops.

Numerical predictions show a qualitative agreement with experimental observations. In particular, the shape of the cavity is captured in most cases, whereas a common trend to overestimate the extent of vapor regions on the blade surface is noted. Larger values of the α_v threshold used would improve the agreement with experimental data. Related to this, the analysis of predicted cavity volume defined as the integral of vapor fraction values over the whole computational domain is more rigorous. For the case addressed in Fig. 16, cavity volume values of $3.75e-6$ and $3.86e-5$ m^3 are reported by two participants (no experimental data available). Similarly, predicted cavity area defined as the integral of vapor fraction values over blade surface grid cells are in the range $3.84e-5$ to $1.33e-3$ m^2 (four results submitted, compared to a measured value of $7.13e-4$ m^2 , see Pereira et al (2004).

Let us now consider the differences between the various codes for the unsteady flow conditions when the propeller operates in a non-homogeneous wakefield. The differences in modelling the inflow to the propeller are recognized here as a major source for these different results. In some calculations, too strong a numerical dissipation weakens the wakefield in the propeller region (see Fig. 11). As a result, the propeller blade does not reach the maximum loading and the corresponding calculated cavity patterns tend to be underestimated compared to the experimental observations, as shown in Figs. 14 and 15. In this case, predicted blade cavity areas are in a relatively narrow range, $1.80e-4$ to $9.84e-4$ m^2 (maximum value during propeller revolution) compared to a measured value of $8.21e-4$ m^2 . To the contrary, the scatter of predicted cavity volume values is even larger

than in uniform flow, with estimates between $2.8e-7$ and $1.41e-5$. This aspect raises a question on the reliability of current CFD models to predict dynamic cavitation effects like pressure fluctuations, noise and erosion.

In the case of a propeller operating in a wakefield, numerical results are furthermore affected by the different meshing techniques used to impose the prescribed axial wake. Models based on a sliding mesh approach where the measured axial wake is imposed as inlet condition are compared to models where the whole computational domain is rotating with the propeller, and an idealized analytical definition of the wakefield is used.

A grid refinement study was beyond the scope of the propeller test case. Nevertheless, results presented by some organizations comparing solutions obtained using different grids reveal a large variation in the predicted cavity patterns. In particular, the correct modelling of cavitation requires that flow regions where vapor generation, transport and destruction occur are discretized with a much higher grid density than typically needed for the non-cavitating flow outside the inner boundary layer. LES simulations resolve (not surprisingly) more structures in time and space than RANS calculations. Transient cavitation results show that two-phase flow details like the process of leading-edge detachment are in this case accurately described by LES. Moreover, results comply with the non-periodic nature of cavitation usually observed on model scale propellers. From the workshop results it appears that LES-based models are promising tools to investigate the risk of cavitation erosion. It should however be noted that the computational time needed for the propeller computations with Chalmers' OPENFOAM is of the order of CPU months.

For a further analysis of the differences in computed results, reference is made to the NACA0015 2D test case, that served as one of the three test cases for the Workshop. Results on this 2D foil in a uniform inflow showed a similar scatter in results for the cavity extent and dynamics as found on the propeller. Some of the findings from the 2D foil are summarized here:

- It was shown that turbulence models can change the character of the cavity. Computations with STAR-CD for instance showed that the character of the sheet cavity could change from a non-shedding oscillating cavity with a frequency of approx. 4Hz to an unstable shedding cavity with a dominant frequency of 14 Hz. This difference was obtained by using a $\kappa-\epsilon$ turbulence model for the first, and an RNG $\kappa-\epsilon$ model for the second case. Computations with COMET showed that using the RNG $\kappa-\epsilon$ model showed stronger dynamics than the $\kappa-\omega$ model.
- The choice of the cavitation model (Sauer's versus Kunz model) was shown to cause a clear difference in the thickness of the re-entrant jet.
- The grid density was shown to have an important effect on the extent and volume of sheet cavitation from a systematic study with FreSCo. It was

concluded that the grid should not only be refined in the wetted boundary layer flow, but also at the cavity interface. Too much numerical dissipation seems to result from too coarse a grid. It is believed that the grid density is likely to be the most important source for differences between properly verified codes.

- Based on the workshop results, it is hypothesized that differences between results are to a large extent caused by grid density and numerical dissipation and to a lesser extent by the different turbulence models (and probably by different cavitation models as well). This hypothesis is supported by the results obtained with the non-viscous Euler solver CATUM in e.g. Schmidt et al. (2008). In this paper, the authors show that the cavitating vortices in the wake of a triangular prism are predicted qualitatively well and that the location of the impact pressures caused by the breaking up of the cavitating vortex corresponds to the experimentally determined locus of erosive damage. These authors conclude that the mechanism governing the cavity dynamics is "strongly inertia controlled".

7. CONCLUSIONS AND RECOMMENDATIONS

Results of computational studies submitted to the VIRTUE 2008 Workshop provide a broad view on state-of-the-art propeller cavitation models by RANS, LES and BEM. Performances of computational models have been benchmarked against a common test-case addressing the INSEAN E779A propeller in uniform flow and in a given wakefield.

Considering the open water performance, it is concluded that the uncertainty in predicting thrust and torque is lower than 5%, this latter value being the standard deviation of the differences between measurement and computed value. It is also noted that the trend of the open water performance with J is properly predicted.

The predicted cavity extents for both steady and unsteady inflow do qualitatively agree with experimental observations, whereas important quantitative differences are observed. These differences in cavity extent and volume render computations not sufficiently suitable for a prediction of radiated pressure fluctuations nor predictions of cavitation erosion. It is concluded that predictions of pressure fluctuations from a potential flow BEM code (in this case the INSEAN PFC code) give, so far, the most reliable results.

The differences in results of the various CFD codes are likely to be caused primarily by a lack of grid density and/or too much numerical dissipation in the vicinity of the cavity-fluid interface. In addition to these effects, turbulence and cavitation models were also demonstrated to affect the cavity extents and dynamics.

Related to the issue of grid resolution, is the finding that predictions by LES solve time and space scales better than RANS. The capability of an LES code to describe

important two-phase flow structures has been demonstrated. This resolution in predicting flow phenomena appears useful for the assessment of erosion risks.

The modelling of a non-homogeneous inflow was shown to represent a critical issue. The correct interpolation of velocity between fixed and rotating grid blocks when a sliding mesh technique is used and the numerical diffusion in the wakefield are of primary importance when modelling a propeller operating in a hull wake by CFD.

The issue of grid resolution in the cavitating flow region and numerical dissipation were demonstrated to be of great importance for the prediction of cavity extent and dynamics. The VIRTUE 2008 Rome Workshop demonstrated that this issue is generally not yet under control. Numerical uncertainty studies are required before firm conclusions about the adequacy of turbulence and cavitation models can be drawn. The 2D NACA0015 foil test case can be regarded as a starting point.

ACKNOWLEDGEMENTS

The authors wish to thank workshop participants who made possible this paper providing detailed reports of their computational studies: Rickard Bensow, Alexandre Capron, Dieke Hafermann, Robert Kunz, Da-Qing Li, Jay Lindau, Jussi Martio, Benoit Tartinville, Tuomas Sipila. Part of work described in this paper has been performed in the Framework of the Eu-FP6 VIRTUE Project, grant TIP5-CT-2005-516201.

REFERENCES

- Atlas, M. (ed.) (2004). First International Conference on Technological Advances in Podded Propulsion. School of Marine Science and Technology, University of Newcastle, UK.
- Fluent Inc. (2006). FLUENT 6.3 User's guide.
- Bensow R.E., Huuva, T., Bark, G. & Liefvendahl, M. (2008). 'Large Eddy Simulation of Cavitating Propeller Flow.' Proceedings of the twenty-seventh ONR Symposium on Naval Hydrodynamics, Seoul, Corea.
- Delannoy, Y. & Kueny, J. L. (1990). 'Two phase flow approach in unsteady cavitation modelling.' Cavitation and Multiphase Flow Forum, ASME-FED 98, pp. 153-158.
- Kunz, R.F., Boger, D.A., Stinebring, D.R., Chyczewski, T.S., Lindau, J.W., Gibeling, H.J., Venkateswaran, S., & Govindan, T.R. (2000). 'A Preconditioned Navier-Stokes Method for Two-Phase Flows with Application to Cavitation Predication.' Computers and Fluids 29, pp. 849-875.
- Li, D-Q and Grekula, M. (2008). 'Prediction of Dynamic Shedding of Cloud Cavitation on a 3D Twisted Foil and Comparison with Experiments.' Proceedings of the 27th ONR Symposium on Naval Hydrodynamics, Seoul, Korea.
- Merkle, C. L., Feng, J. & Buelow, P. E. O. (1998). 'Computational modeling of the dynamics of sheet cavitation.' Proceedings of the Third International Symp. on Cavitation, CAV '98, Grenoble, France.
- NUMECA International s.a (2006). FineTM/Turbo 7.4 User Manual.
- Pereira, F., Salvatore, F. & Di Felice, F. (2004a). 'Measurement and Modelling of Propeller Cavitation in Uniform Inflow.' Journal of Fluids Engineering 126, pp. 671-679.
- Pereira, F., Salvatore, F., Di Felice, F. & Soave, M. (2004b). 'Experimental Investigation of a Cavitating Propeller in Non-Uniform Inflow.' Proceedings of the twenty-fifth ONR Symposium on Naval Hydrodynamics, St. John's, Newfoundland, Canada.
- Salvatore, F., Pereira, F., Felli, M., Calcagni, D. & Di Felice, F. (2006a). Description of the INSEAN E779A Propeller Experimental Dataset. Technical Report INSEAN 206-085, Rome, Italy.
- Salvatore, F., Testa, C., Ianniello, S. & Pereira, F. (2006b). 'Theoretical Modelling of Unsteady Cavitation and Induced Noise.' Proceedings of the Sixth International Symp. on Cavitation, CAV 2006, Wageningen, The Netherlands.
- Sánchez-Caja, A., Rautheimo, P., Salminen, E. & Siikonen, T. (1999). 'Computation of the Incompressible Viscous-Flow Around a Tractor Thruster Using a Sliding-Mesh Technique.' Proceedings of the seventh International Conference on Numerical Ship Hydrodynamics, Nantes, France.
- Sauer, J. (2000). Instationär kavitierende Strömungen - Ein neues Modell, basierend auf Front Capturing (VoF) und Blasendynamik. Doctoral Thesis, University of Karlsruhe, Germany (in German).
- Schmidt, S.J., Sezal, I.H., Schnerr, G.H. and Thalhamer, M. (2008). "Numerical analysis of shock dynamics for detection of erosion sensitive areas in complex 3-D flows", Proceedings of the WIMRC Forum 2008, Warwick University, Warwick, United Kingdom.
- Singhal, A. K., Athavale, M. M., Li, H. & Jiang, Y. (2002). 'Mathematical Basis and Validation of the Full Cavitation Model.' Journal of Fluids Engineering 124, pp.617-624.
- Streckwall, H., & Salvatore, F. (2008). 'Results from the Wageningen 2007 Workshop on Propeller Open Water Calculations Including Cavitation.' Proceedings of the RINA Symposium on CFD Models, London, UK.
- Vaz, G. & Hoekstra, M. (2006). Theoretical and Numerical Formulation of FRESKO Code. Technical Report 18572-WP4-2, MARIN.
- Vorhölter, H., Schmode, D. & Rung, T. (2006). 'Implementation of Cavitation Modeling in FRESKO.' Proceedings of the NuTTS Symposium, Varna, Bulgaria.